Current-voltage characteristic and stability in resonant-tunneling *n*-doped semiconductor superlattices

A. Wacker,* M. Moscoso, M. Kindelan, and L. L. Bonilla
Escuela Politécnica Superior, Universidad Carlos III de Madrid, Butarque 15, 28911 Leganés, Spain
(Received 26 April 1996)

We review the occurrence of electric-field domains in doped superlattices within a discrete drift model. A complete analysis of the construction and stability of stationary field profiles having two domains is carried out. As a consequence, we can provide a simple analytical estimation for the doping density above which stable domains occur. This bound may be useful for the design of superlattices exhibiting self-sustained current oscillations. Furthermore we explain why stable domains occur in superlattices in contrast to the usual Gunn diode. [S0163-1829(97)08504-4]

I. INTRODUCTION

Electrical transport in semiconductor superlattices (SL's) has attracted much interest during the past years due to the very different interesting properties related to the artificial band structure. One of these features is the occurrence of stationary electric-field domains which have already been reported in Ref. 1. Due to advanced growing facilities and experimental techniques the complicated structure of the current-voltage characteristics which exhibits several branches, roughly equal to the number of quantum wells, could be resolved during the past decade.[2–7] In these experiments it was demonstrated that the different branches are connected to the formation of two domains with different values of the electric-field inside the sample. Depending on the conditions, stable stationary field domains and traveling domain boundaries may occur. In the latter case, the dynamics of the electric field domains gives rise to time-dependent oscillations of the current.[8–11]

Early approaches towards a modeling of these phenomena have been performed within a continuum model including strong diffusion[12] and with the help of an equivalent circuit.[13] During the past years it has been shown theoretically that the observed phenomena can be fairly well reproduced by models which essentially combine the discrete Poisson-equation and rate equations for the carrier densities in the different quantum wells.[14–16] Also the time-dependent current oscillations could be recovered in these models.[15,17,18] A prediction of spatiotemporal chaos in resonant-tunneling superlattices under dc+ac voltage bias has been made on the basis of the discrete drift model.[19] The influence of growth-related imperfections on the SL behavior has been studied in Ref. 20. Some of these phenomena may also be described by discrete models with Monte Carlo dynamics incorporating single-electron tunneling effects (which are important for slim superlattices and give rise to additional oscillations of the current[21,22]).

In this paper we want to explain *how* these complicated phenomena are generated by such models. This provides a deeper insight into the basic mechanisms and helps to classify the results of various experiments and computer simulations. In particular we want to give an answer to the following questions: How is it possible to understand the appearance of the complicated structure of the current-voltage characteristic? What are the conditions for stability and oscillations and how can they be understood? What is the main difference to the Gunn diode, where hardly any stable domain states are observed?

The paper is organized as follows: The model we use is described in the second section. The third section shows how the complex stationary current-voltage characteristic changes as the doping increases. In the fourth section we investigate the stability of the stationary states and prove an explicit criterion for the occurrence of stable domain states. The last section contains our conclusions and the Appendix is devoted to a proof that no self-sustained oscillations appear for a small product of doping times the number of SL periods. When the doping density lies in the range between these two stability boundaries, the model exhibits self-sustained oscillations. Results concerning self-sustained oscillations of the current are presented in a companion paper,[23] where a direct comparison with experimental data is made.

II. THE MODEL

We consider a semiconductor superlattice where the lateral extension of wells and barriers is much larger than the total length of the SL, so that single-electron tunneling effects (see, e.g., Ref. 21) are negligible. The quantum wells (QW's) are weakly coupled and the scattering times are much shorter than the tunneling time between adjacent QW's. Thus it makes sense to consider the electrons to be localized within the QW's and in local equilibrium at the lattice temperature. The current is mainly determined by the resonances between the different energy levels in the QW's, which we denote by Ci, $i=1,2,\ldots$, in order of increasing energy counted from the bottom of the conduction band. For the biases of interest here, there are three important resonances $C1C1$, $C1C2$, and $C1C3$. If the intersubband relaxation is also fast with respect to the tunneling, in practice only the lowest subband is occupied. In this case it is a reasonable approximation to consider the QW's as entities characterized by average values of the electron density $\widetilde{n}_i$ in the ith QW (in units cm^{-2}) and the electric field $\widetilde{E}_i$ between wells i and $i+1$, with $i=1,\ldots N$. For sufficiently high elec-

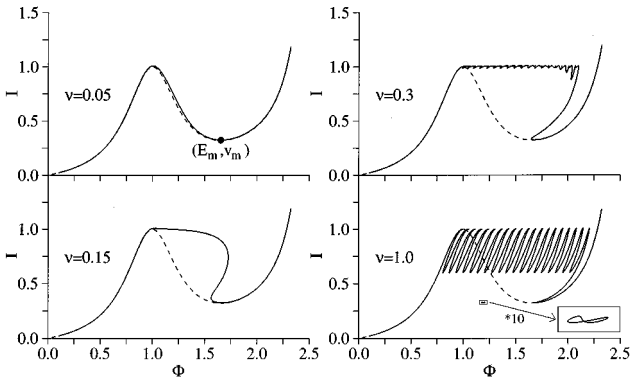

FIG. 1. Current-voltage characteristics for $c=0.01$ and $N=20$ and different values of ν. The full line denotes the states where the electric field E_i is strictly monotone increasing in i. For $\nu=1.0$ there appear additional branches with nonmonotonic field profiles E_i. They are isolated from the stationary branches having increasing field profiles. We have shown one such branch, which has also been blown up for the sake of clarity. The dotted line is the $v(E)$ curve used throughout this paper.

tric fields, the electrons tunnel only in the forward direction and we can describe the dynamical behavior of $\tilde{n}_i$ by the rate equation,

$$\frac{d\tilde{n}_i}{d\tilde{t}}=\frac{1}{\tilde{l}}[\tilde{v}(\tilde{E}_{i-1})\tilde{n}_{i-1}-\tilde{v}(\tilde{E}_i)\tilde{n}_i], \tag{1}$$

where $\tilde{l}$ is the superlattice period and $\tilde{v}(\tilde{E})/\tilde{l}$ is the average electron tunneling rate for the local field. $\tilde{v}(\tilde{E})$ has a peak at certain values of the electric field connected to resonant tunneling $C1C1$, $C1C2$, and $C1C3$. In this paper we shall be concerned with phenomena occurring at fields higher than the first resonant peak $C1C2$, so that we shall omit the miniband peak $C1C1$ in our tunneling rate $v(E)$; see the curve plotted in Fig. 1 by a dashed line. Phenomena at lower fields have been studied by adding the $C1C1$ peak to our curve.[24] The electric fields must fulfill the Poisson equation averaged over one SL period,

$$\tilde{E}_i-\tilde{E}_{i-1}=\frac{q}{\epsilon}(\tilde{n}_i-\tilde{N}_D), \tag{2}$$

where ϵ, q, and $\tilde{N}_D$ are the average permittivity, the charge of the electron, and the donor density per SL period (in units cm^{-2}), respectively. By differentiating Eq. (2) with respect to time we obtain Ampère's law for the total current density $\tilde{J}(\tilde{t})$:[17]

$$\epsilon\frac{d\tilde{E}_i}{d\tilde{t}}+\frac{1}{\tilde{l}}\tilde{v}(\tilde{E}_i)[q\tilde{N}_D+\epsilon(\tilde{E}_i-\tilde{E}_{i-1})]=\tilde{J}, \tag{3}$$

where $i=1,\ldots,N$. Typically the experiments are performed with a constant dc voltage bias $\tilde{\Phi}$ yielding

$$\tilde{l}\sum_{i=1}^{N}\tilde{E}_i=\tilde{\Phi}. \tag{4}$$

Notice that there are $2N+2$ unknowns:

$$\tilde{E}_0,\tilde{E}_1,\ldots,\tilde{E}_N,\tilde{n}_1,\ldots,\tilde{n}_N,\tilde{J}$$

and $2N+1$ equations, so that we need to specify one boundary condition for $\tilde{E}_0$ plus an appropriate initial profile $\tilde{E}_i(0)$. The boundary condition for $\tilde{E}_0$ (the average electric field *before* the SL) can be fixed by specifying the electron density at the first site, $\tilde{n}_1$, according to (2). In typical experiments the region before the SL has an excess of electrons due to a stronger n doping there than in the SL.[8–11] Thus it is plausible assuming that there is an excess number of electrons at the first SL period measured by a dimensionless parameter $c>-1$:

$$\tilde{n}_1=(1+c)\tilde{N}_D. \tag{5}$$

c has to be quite small because it is known that a steady uniform-electric-field profile is observed at low laser illumination in undoped SL.[8,15,17] This observation allows us to infer the electron tunneling rate $v(E)$ directly from measured current-voltage data.[15] Another possibility is to derive $v(E)$ from simple one-dimensional quantum-mechanical calculations of resonant tunneling, as was done by Prengel *et al.*[14] They used a more complicated discrete model with two electron densities corresponding to the populations of the two lower energy levels of each QW. Their model reduces to a form of ours when the large separation between the time scales of phonon scattering, resonant tunneling, and dielectric relaxation is taken into account.

For the calculations that follow, it is convenient to render Eqs. (3)–(5) dimensionless by adopting as the units of electric field and tunneling rate the values at the $C1C2$ peak of the $v(E)$ curve, $\tilde{v}(\tilde{E})$, $\tilde{E}_M$, and $\tilde{v}_M$ (about 10^5 V/cm and 10^3 cm/s, respectively, for the sample of Ref. 10). Like in Ref. 17, we set

$$E_i=\frac{\tilde{E}_i}{\tilde{E}_M},\quad n_j=\frac{q\tilde{n}_i}{\epsilon\tilde{E}_M},\quad I=\frac{\tilde{J}\tilde{l}}{q\tilde{N}_D\tilde{v}_M},$$

$$v=\frac{\tilde{v}}{\tilde{v}_M},\quad t=\frac{q\tilde{N}_D\tilde{v}_M\tilde{t}}{\epsilon\tilde{E}_M\tilde{l}},\quad \phi=\frac{\tilde{\Phi}}{N\tilde{E}_M\tilde{l}}. \tag{6}$$

We obtain the dimensionless equations

$$\frac{dE_i(t)}{dt}=I(t)-\left(1+\frac{E_i-E_{i-1}}{\nu}\right)v(E_i) \tag{7}$$

for $i=1,\ldots N$,

$$\phi=\frac{1}{N}\sum_{i=1}^{N}E_i(t), \tag{8}$$

and the boundary condition

$$E_0(t)=E_1(t)-c\nu. \tag{9}$$

The dimensionless parameter ν, is defined by

$$\nu=\frac{\tilde{N}_Dq}{\epsilon\tilde{E}_M}, \tag{10}$$

which yields about 0.25 for the SL used in the experiments.[10,11] The constant voltage condition (8) determines the current to be

$$I(t)=\frac{1}{N}\sum_{i=1}^{N}\left(1+\frac{E_i-E_{i-1}}{\nu}\right)v(E_i). \tag{11}$$

With the choice (6), the dimensionless tunneling rate $v(E)$ has a maximum at $E=1$ with $v(1)=1$. Throughout this paper we use the function $v(E)$ which is plotted in Fig. 1 by a dashed line. Besides having a maximum $v(1)=1$, it has a minimum at $E_m\approx 1.667$ with $v(E_m)=v_m\approx 0.323$. Nevertheless nearly all of the features discussed in the following are independent of the exact shape of the function $v(E)$. We only impose the restrictions that $v(E)>0$ for $E>0$ and the existence of a minimum at $E_m>1$.

For any $\phi>0$, we shall assume that the initial electric-field profile is strictly positive and that the electron density is non-negative: $E_i(0)>0$, $n_i(0)\equiv E_i(0)-E_{i-1}(0)+\nu\geq 0$, $\forall i$. This is reasonable unless ϕ is close to zero (but then the $C1C1$ peak in the tunneling-rate curve should be restored) or the boundary conditions are unrealistic. From the equations and our assumption on the initial field profile, it follows that $E_i>0$ and $n_i\equiv E_i-E_{i-1}+\nu\geq 0$ for all positive times. The model equations have interesting properties concerning the monotonic behavior of the electric fields with respect to the QW number. These are summarized in the following lemmas:

Lemma 1. *If the fields of two adjacent QW's are identical, i.e., $E_k=E_{k-1}$ holds for some k with $2\leq k\leq N$, there is at least one i from $1\leq i\leq k$ with $E_i=E_{i-1}$ and $d(E_i-E_{i-1})/dt\neq 0$. For $c=0$ there is the additional possibility that $E_0=E_1=\ldots=E_k$ holds.*

Lemma 2. *If $c\geq 0$ and the field distribution is monotone increasing at $t=0$ [$E_i(0)\geq E_{i-1}(0)$, $\forall i$], it will keep this property for all later times $t>0$. (For $c\leq 0$, the same holds for a decreasing field distribution.)*

Both lemmas can be easily proved. If $E_k=E_{k-1}$ holds, Eq. (7) gives

$$\frac{d}{dt}(E_k-E_{k-1})=\frac{E_{k-1}-E_{k-2}}{\nu}v(E_{k-1}). \tag{12}$$

Therefore $d(E_k-E_{k-1})/dt=0$ implies $E_{k-1}=E_{k-2}$. Then we may repeat the argument until we either find an $i\in\{2,3,\ldots k\}$ with $E_i=E_{i-1}$ and $d(E_i-E_{i-1})/dt\neq 0$ or we find $E_1=E_0$ which violates the boundary condition for $c\neq 0$. This proves lemma 1. Lemma 2 is proved by contradiction. Assume that at $t\geq 0$ the sequence $\{E_i\}$ is increasing but $E_k=E_{k-1}$ and $d(E_k-E_{k-1})/dt<0$ for some k. Then Eq. (12) yields $E_{k-1}-E_{k-2}<0$ in contradiction to the assumed increasing behavior at t. In order to understand the properties of the current-voltage characteristics, we will use repeatedly these basic lemmas in what follows.

III. STATIONARY STATES

In this chapter we want to explain how the complex domain structures found experimentally and from computer simulations[5,7,14,15] are generated by this simple model. We denote the electric-field profile and the current density of stationary states by E_i^* and I^*, respectively. An easy way to construct the stationary profiles is to fix I^*, find out the corresponding electric-field profile $\{E_i^*\}, i=1,\ldots,N$, calculate their voltage as a function of I^*

$$\phi(I^*)=\frac{1}{N}\sum_{i=1}^{N}E_i^*(I^*). \tag{13}$$

The field profile must fulfill the equation

$$E_{i-1}^*=E_i^*+\nu\left(1-\frac{I^*}{v(E_i^*)}\right)=:f(E_i^*,I^*), \tag{14}$$

which was also used in Ref. 15. The boundary condition implies

$$v(E_1^*)=\frac{I^*}{c+1}\Leftrightarrow f(E_1^*,I^*)=E_1^*-c\nu, \tag{15}$$

which has three solutions E_1^* for a known fixed value of the current on the interval $(1+c)v_m<I^*<1+c$.

In order to understand the properties of the stationary profiles we will now investigate the behavior of the set $\{E_i^*\}$ as a function of E_1^*. At first we restrict ourselves to $c>0$ and increasing field profiles. To construct $\{E_i^*\}$, we have to invert the function $f(E,I^*)$ for a fixed value of I^*. Its derivative is

$$\frac{\partial f(E,I^*)}{\partial E}=1+\nu\frac{I^*}{v(E)^2}\frac{dv(E)}{dE}. \tag{16}$$

With the restriction to increasing field profiles, we can always obtain E_i^* for $E_1^*\geq E_m$ because $dv/dE>0$ and $f(E_mI^*)<E_m$ holds. If $E_1^*<E_m$, Eq. (15) implies $I^*\leq 1+c$ and we find that $f(E,I^*)$ is strictly monotone increasing for all E if

$$\frac{1}{\nu}\geq\max\left\{\frac{-(1+c)}{v(E)^2}\frac{dv(E)}{dE}\right\}, \tag{17}$$

yielding a condition which only depends on the $v(E)$ relation but is not dependent on I. For our function $v(E)$ this yields $\nu\leq 0.195/(1+c)$. In this case the function $f(E,I^*)$ (I^* fixed) is always invertible. Then we can find a unique field profile parametrized by the point E_1^*. Since we have three possible solutions E_1^* of (15) for each given $I^*/(1+c)\in(v_m,1)$, there are three different voltages ϕ for each value of the current in this range. The function $\phi(I^*)$ is thus three valued, which means that by inverting it we obtain an N- or a Z-shaped current-voltage characteristic as shown in Fig. 1 for $\nu=0.05$ and $\nu=0.15$, respectively. Both types can be easily understood: When the doping density ν is low, Eq. (14) shows that $E_i^*\approx E_1^*$ holds. Thus, the field profile is nearly uniform and the current-voltage characteristics follow the $v(E)$ curve as shown in Fig. 1 for $\nu=0.05$. This is physically obvious as there are few charges present inside the sample. For larger values of ν the values E_i^* may strongly deviate from E_1^* with increasing i, if E_1^* is not a fixed point of $f(E,I^*)$ (which is the case for $c=0$ Ref. 15). Let us denote by $E^{(1)}(I)<E^{(2)}(I)<E^{(3)}(I)$ the three solutions of $v(E)=I$ for a given $I\in(v_m,1)$ which are the fixed points of

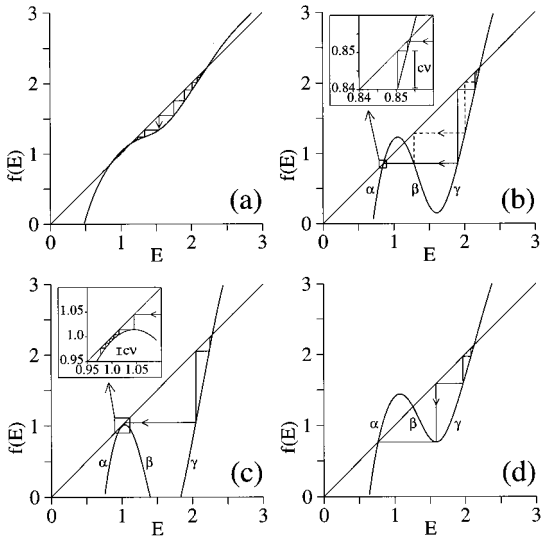

FIG. 2. $f(E,I)$ and a trajectory E_i indicating decreasing i for various doping densities and currents. (a) $\nu=0.15$, $I=0.8$. (b) $\nu=1.0$, $I=0.8$. (c) $\nu=1.0$, $I=1.008$. (d) $\nu=1.0$, $I=0.599=I_c$.

Eq. (14). If ϕ is small and $c>0$, E_1^* is on the first branch of $v(E)$ and the values E_i^* tend to $E^{(1)}(I^*)$. When ϕ is larger and E_1^* is located on the second branch of $v(E)$, the sequence E_i^* leaves the neighborhood of $E^{(2)}(I^*)$ and then approaches $E^{(3)}(I^*)$ on the third branch of $v(E)$ if ν is large enough. This is shown in Fig. 2(a). In this case the voltage is basically determined by the fixed point $E^{(3)}(I^*)$. Since $dE^{(3)}(I)/dI>0$, this branch of stationary solutions may exhibit a range of positive differential conductance leading to the Z shape. This effect is more pronounced for longer superlattices with many wells N and also for larger values of c.

For larger doping ν the condition (17) is violated and the function $f(E,I)$ may not be invertible for some current I. In this case there can be more than one possible E_{i+1} following a given E_i. Then the current-voltage characteristic can no longer be unambiguously parametrized by the point E_1^*. In general $f(E,I)$ has three different branches for a certain interval of I^*, as shown in Fig. 2(b). Let us call branch α that having $\partial f/\partial E>0$ for low E, branch β has $\partial f/\partial E<0$, and branch γ again has $\partial f/\partial E>0$ but for larger E.

Let us explain how to construct different stationary field profiles for a given value of the current I^*. We shall assume that the profiles are increasing, $E_{i+1}^*\geqslant E_i^*$, $\forall i$. First of all, E_1^* may be located on branch γ of $f(E,I^*)$, and so will all successive fields E_i^*. This profile will have the largest possible voltage for the same I^*. Second, E_1^* may be located on branch β, which implies that all successive E_i^* of an increasing field profile have to be on branch γ. The corresponding voltage is smaller than that of the previously described branch but larger than those stationary solution branches that we analyze next.

If E_1^* is on branch α, we may have E_i^*, $i=1,\ldots,j-1$, $(j=2,\ldots,N)$ on branch α, and E_j^* either on branch β or on branch γ. We obtain a different branch of stationary solutions for each such possibility. Let us denote by (j,β) or (j,γ) the solution branch having E_j^* either on branch β or

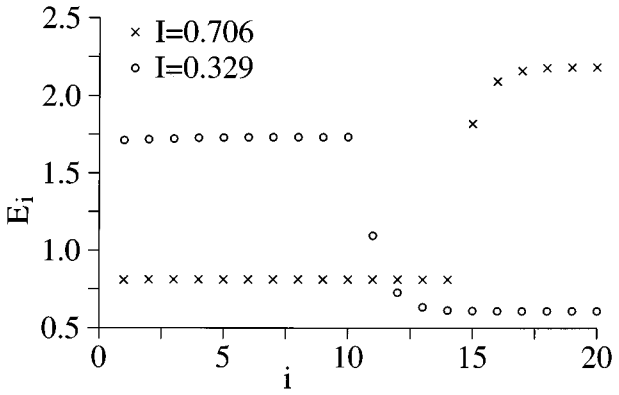

FIG. 3. Different stationary electric-field profiles for $c=0.01$, $\nu=1.0$, $\phi=1.2$, and $N=20$. The crosses mark a state of the connected branch from Fig. 1 ($\nu=1.0$) while the circles mark a state belonging to the isolated branch.

γ, respectively, and E_i^*, $i=1,\ldots,j-1$ on branch α. In Fig. 2(b) a solution (j,β) is shown by a dashed line and a solution (j,γ) by a full line. Clearly $j=1$ corresponds to the possibilities discussed above. Finally, we have one solution where all field values are on branch α which we denote by $(N+1,\gamma)$. In order of increasing voltages, we have

$$\phi_{(N+1,\gamma)}(I^*)\leqslant\phi_{(N,\beta)}(I^*)\leqslant\phi_{(N,\gamma)}(I^*)\leqslant\ldots\leqslant\phi_{(1,\beta)}(I^*)\leqslant\phi_{(1,\gamma)}(I^*),$$

corresponding to $2N+1$ different stationary solution branches with the same current I^*. They can be observed in Fig. 1 for $\nu=1.0$ and $I^*=0.8$. Notice that the branches $(j+1,\gamma)$ and (j,β) coalesce at a current $I^*\in(1,1+c)$ which is roughly independent of ν [see Fig. 2(c)]. The branches (j,β) and (j,γ) coalesce at a lower current I_c which decreases as ν increases [see Fig. 2(d)]. The current-voltage characteristic curve is thus connected as shown in Fig. 1 ($\nu=1.0$).

The field profile of the solution branch $(15,\gamma)$ is depicted by the crosses in Fig. 3. One can clearly identify two regions $1\leqslant i<j$ and $j<i\leqslant N$, where the electric field E_i^* is roughly constant and close to a fixed point with $v(E_i^*)\approx I^*$. In between there is a transition layer, the domain boundary, consisting of only a few wells. These type of states we call domain states. A shift of the domain boundary by one well only changes the voltage as long as the transition layer does not extend to one of the contacts. As the stationary solutions resulting from a one-well shift are very similar, the domain branches in the current-voltage characteristics look alike, as can be seen in Fig. 1 ($\nu=1.0$). The slope of the different domain branches in Fig. 1 may vary from branch to branch. The high-field domain corresponding to far right branches has a much larger extension than the low-field domain. Then the slope of these branches in Fig. 1 will be closer to the slope (conductivity) of the third branch of the curve $v(E)$. Similarly the slope of far left branches in Fig. 1 will be closer to the slope of the first branch of $v(E)$. The larger the difference in slope between first and third branches of $v(E)$ is, the larger the variation in the slope of the branches in Fig. 1 will be.

Note that the domain states are not very sensitive to the exact type of boundary conditions if two conditions are fulfilled:

(1) The boundary conditions must allow for the existence of a roughly constant field distribution $E_i^* \approx E^{(1)}$ and $E_i^* \approx E^{(3)}$ probably after a short contact layer of some wells.

(2) The domain boundary must be located sufficiently deep inside the sample, so that it does not collide with the contact layer.

As ν decreases, the solution branches become shorter and eventually disappear if I_c becomes larger than $(1+c)$, which happens if the inequality (17) holds. The stationary domain structures are seen for narrow current intervals about $I^*=1$ for intermediate doping as shown in Fig. 1 ($\nu=0.3$). Another complex feature can be found here for larger voltages where extra wiggles appear. They occur if E_1^* crosses the value 1, yielding an additional maximum in I^*.

Except for the fundamental question of stability, we have now understood the morphology of the complicated current-voltage characteristic curve shown in Fig. 1, its changes with doping, and its relation with the electric-field profile. The very same features occur in the more complicated model of Prengel *et al.*[14,18] as shown numerically in Ref. 25.

So far we have restricted ourselves to increasing field profiles. Therefore we could only find domain states where the high-field domain is located at the receiving contact and the domain boundary is an accumulation layer. Nevertheless, this is not the full story. For sufficiently large ν other solutions are also possible, even for $c>0$. A typical such field profile is depicted by circles in Fig. 3. The field starts on branch γ of the function $f(E,I^*)$ and first increases with the QW index towards the third fixed point $E^{(3)}(I^*)$. At a certain QW j the field jumps down to either branches α or β, and then decreases down towards the first fixed point $E^{(1)}(I^*)$. Of course ν has to be large enough for these jumps down to be possible. Thus these field profiles have a high-field domain located at the injecting contact and the domain boundary separating this domain from a low-field domain is a depletion layer. Numerical investigation shows that these stationary states are stable and that they can be reached from many initial conditions. Lemma 2 tells us that the initial field distribution cannot be monotone increasing in the well index (like the solutions of the connected branch discussed before), for otherwise the field distribution would keep this property for all times. Thus, these different stationary solutions are not connected to the branches dicussed before (having an increasing field profile) but form many additional isolated closed curves or ''isolas.''[26,27] A typical isolated curve is shown inside the frame in Fig. 1 for $\nu=1.0$, which is also blown up to an enlarged scale for the sake of clarity.

A special situation arises if $c=0$ holds. In this case the branches of increasing and decreasing field profiles become connected and there appears much additional degeneracy leading to an extremely complicated structure as observed in Ref. 15.

IV. STABILITY OF THE STATIONARY STATES

Up to now we have only discussed the existence of stationary states, but not their stability properties. First of all, several stability properties can be established by topological arguments.[26,28] If several branches overlap at a fixed voltage, each second branch has to be unstable by general reasons. For example, the middle branch (exhibiting positive differential conductivity) of the Z-shaped charactistics in Fig. 1 ($\nu=0.15$) has to be unstable. The remaining branches may exhibit further bifurcations. In order to elucidate this, we will perform a linear stability analysis for the states constructed in the previous section. By this method we will prove the following statements:

(A) For large doping $\tilde{N}_D$ exceeding approximately $\epsilon(\tilde{E}_m-\tilde{E}_M)/(q)\tilde{v}_m/(\tilde{v}_M-\tilde{v}_m)$ we find stable domain states.

(B) For very small products $\tilde{N}_D(N-1)$ the almost uniform states are also stable.

For a medium range of doping in between these two limits we find self-generated oscillations as reported in Refs. 10,11, and further discussed in a companion paper.[23]

In order to perform the linear stability analysis, we substitute

$$E_i(t)=E_i^*+e^{\lambda t}\hat{e}_i, \tag{18}$$

$$I(t)=I^*+e^{\lambda t}\hat{j}, \tag{19}$$

in (7) and (9), thereby obtaining

$$\lambda\hat{e}_i=\hat{j}-\frac{I^*v'(E_i^*)}{v(E_i^*)}\hat{e}_i-\frac{v(E_i^*)}{\nu}(\hat{e}_i-\hat{e}_{i-1}), \tag{20}$$

$$\hat{e}_0=\hat{e}_1. \tag{21}$$

These linear equations determine all $\hat{e}_i$ as a function of λ. The fixed bias condition

$$\sum_{i=1}^{N}\hat{e}_i=0, \tag{22}$$

then determines the possible eigenvalues λ. For $\lambda\neq 0$ we now introduce the variable $Y_i=\lambda\hat{e}_i/\hat{j}$ and the parameters

$$b_i=I^*\frac{v'(E_i^*)}{v(E_i^*)}, \quad a_i=\frac{v(E_i^*)}{\nu}, \tag{23}$$

in Eqs. (20) and (21). Then we obtain

$$Y_i=\frac{\lambda+a_iY_{i-1}}{\lambda+a_i+b_i} \quad \text{or} \quad \left\{\begin{array}{c}\lambda+a_i+b_i=0\\ \text{and } Y_{i-1}=-\lambda/a_i\end{array}\right\}, \tag{24}$$

$$Y_1=\frac{\lambda}{\lambda+b_1}. \tag{25}$$

Within the scope of this linear stability analysis, we find that stationary states having all their fields E_i in the positive differential mobility region are stable, which coincides with our physical intuition. This is formulated in the following lemma:

Lemma 3. *If $b_i\geqslant 0$ holds for all $i=1,\ldots N$ the real parts of all eigenvalues have to be negative, i.e., the state is stable. Furthermore the current-voltage characteristic exhibits a positive slope $dI^*/d\Phi$.*

We prove this Lemma by contradiction. Let us assume that $\mathrm{Re}(\lambda)\geqslant 0$ holds with $\lambda\neq 0$. As $b_1\geqslant 0$ we directly find

that $\mathrm{Re}(Y_1)>0$ and $|Y_1-1|\leqslant 1$. In order to satisfy the voltage condition (22) we conclude that there must be at least one Y_j with $\mathrm{Re}(Y_j)<0$. This implies directly that also $|Y_j-1|>1$ must hold. But we find

$$|Y_i-1|=\frac{|a_i(Y_{i-1}-1)-b_i|}{|\lambda+b_i+a_i|}<\frac{|a_i||Y_{i-1}-1|+|b_i|}{|b_i+a_i|}. \tag{26}$$

Given that $|Y_1-1|\leqslant 1$, the last equation implies that $|Y_i-1|\leqslant 1$ for all i. Thus, the case $\mathrm{Re}(\lambda)\geqslant 0$, $\lambda\neq 0$ is excluded.

For $\lambda=0$ we obtain

$$b_1\hat{e}_1=\hat{j} \quad \text{and} \quad (b_i+a_i)\hat{e}_i=\hat{j}+a_i\hat{e}_{i-1}. \tag{27}$$

Therefore all $\hat{e}_i$ have the same phase as $\hat{j}$ and the voltage condition (22) cannot be satisfied unless $\hat{e}_i=0$, $\forall i$ and $\hat{j}=0$, which is the trivial case. In conlusion $\lambda=0$ is not an eigenvalue. Furthermore $\lambda=0$ describes the infinitesimal change along the curve of stationary states. Equation (27) tells us that $\hat{j}/\hat{e}_i\geqslant 0,\forall i$. Identifying $dI^*=\hat{j}$ and $d\phi=\Sigma\hat{e}_i$ we obtain a positive slope of the current-voltage characteristic i.e., $dI^*/d\phi\geqslant 0$.

A. Stability for sufficiently large ν

Lemma 3 establishes that stationary field profiles with $v'(E_i^*)\geqslant 0$, $\forall i$ are linearly stable. These profiles include (i) trivial ones where all the E_i belong to the same branch of $v(E)$, and (ii) profiles where the negative differential mobility region is crossed in a single jump. This means that for a certain value $E_j^*\leqslant 1$ $(1\leqslant j\leqslant N-1)$ there exists $E_{j+1}^*\geqslant E_m$ with $f(E_{j+1}^*,I^*)=E_j^*$. As $f(E,I^*)$ is increasing for $E\geqslant E_m$, the necessary and sufficient condition for the existence of such a value E_{j+1}^* is $f(E_m,I^*)\leqslant E_j^*$. This condition yields

$$(E_m-E_j^*)v(E_m)\leqslant\nu(I^*-v_m). \tag{28}$$

This inequality is first fulfilled for $E_j^*=1$ and $I^*=1$, which are the largest values of the respective quantities for the low-field domain. This gives

$$\nu\geqslant\frac{(E_m-1)v_m}{1-v_m}. \tag{29}$$

If this condition is fulfilled, domain states are possible which cross the negative differential mobility region in a single jump and must be stable therefore.

Nevertheless there can be stable states even for smaller doping ν, as lemma 3 only yields a sufficient and not a necessary condition for stability. For our $v(E)$ curve inequality (29) yields $\nu\geqslant 0.32$. Indeed we do not find any self-sustained oscillations for ν larger than the value $\nu\approx 0.27$, which is somewhat smaller than our estimation. Checking other $v(E)$ curves we have always found oscillations up to a doping roughly $15-40\,\%$ lower than determined by the bound (29). Thus, the bound is not only a sufficient condition but also a reliable rough estimate for doping above which the oscillations disappear.

Transforming to physical units we obtain a surface charge density per well:

$$\widetilde{N}_D\geqslant\frac{\widetilde{v}_m\epsilon(\widetilde{E}_m-\widetilde{E}_M)}{(\widetilde{v}_M-\widetilde{v}_m)q}, \tag{30}$$

which should be a reasonable approximation for the necessary doping density. For the model equations from Prengel,[14] we find $\widetilde{N}_D\geqslant 2.4\times 10^{11}/\mathrm{cm}^2$. Actually, oscillations are found in the model up to roughly $\widetilde{N}_D\approx 10^{11}/\mathrm{cm}^2$ for the regular superlattice and for somewhat higher values for a slight amount of disorder.[20]

If we regard domains with the high-field domain located at the injecting contact the same arguments yield a bound

$$\nu\geqslant\frac{(E_m-1)}{1-v_m} \tag{31}$$

for the existence of stable domains which is larger by a factor $1/v_m$. For our $v(E)$ curve this corresponds to $\nu\geqslant 0.97$. Indeed we have found stable domains with an depletion layer for $\nu=1.0$ as depicted in Fig. 3. This indicates that this type of domain only appears for larger doping. This might explain that two different locations of the high-field domain have been reported in the literature. In Ref. 4 it is found to be located at the injecting contact for a superlattice with $\widetilde{N}_D=8.75\times 10^{11}\ \mathrm{cm}^{-2}$ while in Ref. 29 the high-field domain is located at the receiving contact for a different superlattice with $\widetilde{N}_D=1.5\times 10^{11}\ \mathrm{cm}^{-2}$.

B. Stability for sufficiently small ν

Now we want to show that for sufficiently small doping, the (connected) branches of stationary solutions are stable. Then no self-sustained oscillatory branches bifurcating from them can exist. In order to do this, we note that for very low voltages the stationary state is stable as indicated by lemma 3: all field values of this state are in the range $0<E_i^*<1$. We now increase the voltage and study whether an instability may occur by checking whether it is possible to have $\lambda=i\omega$ with $\omega>0$ for some ϕ. (The case $\lambda=0$ yields the saddle-node bifurcation at the point with $d\phi^*/dI^*=0$, which causes the switching to another branch of the Z-shaped characteristic but typically does not generate any oscillatory behavior.) In the Appendix we show that this is possible only if

$$(N-1)\nu>\min\left\{\frac{\pi(v_l-\nu c_1)}{4c_1},\frac{v_l c_1}{2C(I^*-v_l)c_2}\right\} \tag{32}$$

holds, with

$$v_l=\min\{v_m,(1+c)^{-1}\},$$

$$c_1=I^*\max_{E_l\leqslant E\leqslant E_h}|\partial\ln v(E)/\partial E|,$$

$$c_2=I^*\max_{E_l\leqslant E\leqslant E_h}|\partial^2\ln v(E)/\partial E^2|,$$

$$C=\frac{v_l}{(N-1)\nu c_1}\left[\exp\left(\frac{(N-1)\nu c_1}{v_l-\nu c_1}\right)-1\right].$$

Here E_l,E_h denote the minimal and maximal values of the field for the stationary field profile. Note that for small ν we find $C\to v_l/(v_l-\nu c_1)$ and furthermore the terms νc_1 become negligible. Then the right side no longer depends on

ν and N but only on the shape of $v(E)$ and the parameter c. If ν is smaller and the inequality (32) is violated, no bifurcating oscillatory branches can issue forth from the steady state which is thereby stable.

The bound (32) is far too small due to the rough estimations made during its derivation. Therefore the number itself should not be used for quantitative investigations. Nevertheless we now have shown that the stationary states are stable for low doping and that in the limit of long superlattices the critical doping decreases as $1/N$.

C. Consequences for the continuum limit

With respect to the continuum limit, $N\to\infty$, $\nu\to 0, L:=N\nu<\infty$, we directly find that there exists a minimal length L_m such that the stationary state is linearly stable if $L<L_m$. This lower bound is given by the Eq. (32) with $\nu=0$, $C=1$ and it can be derived directly from the equations valid in the continuum limit, as we shall report elsewhere.[30] Equation (32) and similar bounds derived for other boundary conditions constitute an *explicit* form of the well-known $\tilde{N}_{3D}\tilde{L}$ criterion of the Gunn effect:[31] The dimensionless length L (proportional to doping times the semiconductor length[32,33]) has to be larger than a certain number for the stationary solution to be unstable.

Obviously the upper bound in the doping ν (for the absence of the oscillatory regime) does not exist in the continuum limit ($\nu\to 0$, $N\to\infty$, $L=N\nu$ fixed). The discreteness is essential for the field distribution to jump from the low-field region to the high-field region without any fields exhibiting negative differential $v(E)$ in between (which stabilizes the field distribution). This explains that these stable stationary domains cannot be found in the usual Gunn diode: for large enough dc voltage bias, the Gunn diode may have a stable stationary solution with a large field near the anode.[34,31] However inside the diode there will be a region where the field takes values on the branch of negative differential velocity, which is different from what happens in the SL.

V. CONCLUSIONS

In this paper we have shown how the complex stationary current-voltage characteristic exhibiting domain branches is generated continuously as the doping increases. For low doping the characteristic follows the local $v(E)$ relation. If more charges are present, the characteristic becomes Z shaped. When the doping is even larger, wiggles appear. For each doping the characteristic is connected, and the field profiles of all its different branches are monotone. The different disconnected branches observed experimentally correspond to the stable solution branches of the full stationary current-voltage characteristic. It would be very interesting to investigate whether it is possible to stabilize the unstable branches so that the full characteristic could be observed, as in the case of the double-barrier resonant-tunneling diode.[35,28] Additionally, for large doping there exist isolated branches on the full current-voltage characteristic having nonmonotonic field profiles.

The stability analysis shows that the almost uniform field profile is stable for low doping. The critical doping above which time-periodic oscillations of the current appear is inversely proportional to the sample length for fixed superlattice parameters. This is the same situation as in the famous N_DL criterion for the Gunn diode. For yet larger doping the time-periodic oscillations of the current disappear: there is an upper critical doping above which there appear stable stationary solutions with two electric-field domains (separated by an abrupt domain wall extending almost one period of the superlattice). Obviously, this is not possible for the conventional Gunn diode due to the lack of discretization. It is important to mention that the upper critical doping needed to stabilize stationary domain structures is higher for profiles having depletion layers instead of accumulation layers between the different domains.

This paper gives analytical bounds of the interval of dimensionless doping (proportional to 2D doping over field at resonant tunneling peaks) on which self-sustained current oscillations may exist. To ascertain the influence of the SL parameters and the voltage bias on the current oscillations themselves, a detailed analysis of the dynamics of the model is necessary. This analysis together with experimental verification and predictions on the possibility of tuning the oscillation frequency with applied bias will be presented in a companion paper elsewhere.[23]

Note added in proof. Recently a microscopic calculation[36] revealed that the ansatz for the current $j_{1\to(i+1)}=e\tilde{n}_i\tilde{v}(\tilde{F}_i)$ is justified for large fields (i.e., around and above the $C1C2$ peak) as assumed in Eq. (1). On the other hand, it does not hold for the $C1C1$ resonance, which causes a reduction of the current in the domain branches with respect to the $C1C1$ maximum.

ACKNOWLEDGMENTS

We thank J. Galán, H. T. Grahn, J. Kastrup, M. Patra, F. Prengel, G. Schwarz, E. Schöll, and S. Venakides for fruitful discussions and collaboration on related topics. We thank E. Doedel for sending us his program of numerical continuation AUTO. One of us (A.W.) acknowledges financial support from the Deutsche Forschungsgemeinschaft (DFG). This work has been supported by the DGICYT Grant No. PB94-0375, and by the EU Human Capital and Mobility Programme Contract No. ERBCHRXCT930413.

APPENDIX A: PROOF OF STABILITY FOR SUFFICIENTLY SMALL ν

Here we prove that $\lambda=i\omega$ with $\omega>0$ can be an eigenvalue of the linearized system (20) only if ν is sufficiently large. In order to do this, we assume that a given stationary field profile $\{E_i^c\}$ exhibits $\lambda=i\omega$ with $\omega>0$ and derive several necessary conditions for this. Restricting ourselves to increasing field profiles, E_1^c must either be located on the first or second branch of the $v(E)$ curve, as otherwise the second branch is not reached which is a necessary condition for the instability according to lemma 3. Let us now determine the smallest value E_l and the largest value E_h that the stationary field profile $\{E_i^c\}$ may take. E_l is given by the value of E_1^c on the first branch for which the current takes on its minimal value, $I^*=1$, considering that the field must eventually take values on the second branch of $v(E)$. Equation (15) yields

$v(E_l)=1/(1+c)$ which determines the field $E_l \leqslant 1$. E_h is given by the largest value that E_N^c can take on the third branch of $v(E)$. Noticing that $I^* \leqslant 1+c$ in Eq. (15), we can adopt E_h as the solution of $v(E_h)=1+c$ from the third branch. Thus, E_l and E_h depend only on the $v(E)$ curve and the parameter c but not on the field profile $\{E_i^c\}$. For the sake of convenience we introduce the following quantities:

$$v_l := \min\left\{ v_m, \frac{1}{1+c} \right\}, \tag{A1}$$

$$c_1 := I^* \max_{E_l \leqslant E \leqslant E_h} \left| \frac{\partial \ln v(E)}{\partial E} \right|, \tag{A2}$$

$$c_2 := I^* \max_{E_l \leqslant E \leqslant E_h} \left| \frac{\partial^2 \ln v(E)}{\partial E^2} \right|. \tag{A3}$$

Then we have

$$a_i \geqslant \frac{v_l}{\nu} \quad \text{and} \quad |b_i| \leqslant c_1 \quad \forall i. \tag{A4}$$

In the following we will assume that ν is so small that the function $f(E,I^*)$ (I^* fixed) is always invertible and furthermore

$$a_i + b_i > v_l/\nu - c_1 > 0 \quad \forall i \tag{A5}$$

holds.

For $\lambda = i\omega$, $\omega > 0$, we have $\mathrm{Re}Y_1 > 0$, and $|Y_1 - 1| < 1$. As previously explained in the proof of Lemma 3, there must be a Y_j such that $\mathrm{Re}Y_i \geqslant 0$, $i=1,\ldots,j-1$, and $\mathrm{Re}Y_j < 0$ in order to fulfill the voltage condition. We are going to prove the following result:

Lemma 4. *Let $j>1$ be the index that satisfies $\mathrm{Re}Y_i \geqslant 0$, $i=1,\ldots,j-1$, and $\mathrm{Re}Y_j < 0$.*

(a) If $\omega \leqslant c_1$, we have

$$(j-1)\nu > \frac{\pi v_l}{4Ac_1}, \tag{A6}$$

where A is the maximum of the expressions

$$A_k := \frac{v_l}{(j-k+1)\nu} \sum_{i=k}^{j} \frac{1}{a_i + b_i}, \tag{A7}$$

for $k=2,\ldots j$.

(b) If $\omega > c_1$, we have

$$(j-1)\nu > \frac{v_l c_1}{2B(I^* - v_l)c_2}, \tag{A8}$$

where

$$B := \frac{\mu(\mu^{j-1}-1)}{(\mu-1)(j-1)}, \quad \text{with} \tag{A9}$$

$$\mu := \max_{E_l \leqslant E_i \leqslant E_h} \left\{ \frac{a_i}{|a_i + b_i + ic_1|} \right\}. \tag{A10}$$

Proof:

(a) Let $\omega \leqslant c_1$. In order to prove (A6), we consider how the argument ϕ_i of the complex quantity Y_i is varying with i.

$$\frac{Y_{i-1}}{Y_i} = \frac{|Y_{i-1}|}{|Y_i|} e^{i(\phi_{i-1} - \phi_i)} = \frac{1}{a_i}[i\omega(1 - Y_i^{-1}) + b_i + a_i]. \tag{A11}$$

Therefore we get

$$\phi_{i-1} - \phi_i = \arctan\left(\frac{\omega - \omega \mathrm{Re}(Y_i^{-1})}{b_i + a_i + \omega \mathrm{Im}(Y_i^{-1})} \right). \tag{A12}$$

Furthermore, we have

$$\phi_1 = \arctan\left(\frac{b_1}{\omega} \right). \tag{A13}$$

Straightforward calculations starting from Eq. (24) yield

$$\mathrm{Re}(Y_i) = \frac{\omega^2 + a_i \omega \mathrm{Im}(Y_{i-1}) + a_i(b_i + a_i)\mathrm{Re}(Y_{i-1})}{\omega^2 + (b_i + a_i)^2},$$

$$\mathrm{Re}(Y_i) = \frac{\omega}{b_i + a_i}\mathrm{Im}(Y_i) + \frac{a_i}{b_i + a_i}\mathrm{Re}(Y_{i-1}). \tag{A14}$$

By definition of the index j ($j \leqslant N$), $\mathrm{Re}Y_j < 0$, and $\mathrm{Re}Y_{j-1} \geqslant 0$. Then these equations indicate that $\mathrm{Im}Y_j < 0$ and $\mathrm{Im}Y_{j-1} < 0$. Thus the transition $\mathrm{Re}Y_{j-1} \geqslant 0 \rightarrow \mathrm{Re}Y_j < 0$ occurs across the angle $\phi = -\pi/2$ as we have $-\pi/2 \leqslant \phi_{j-1} < 0$ and $-\pi < \phi_j < -\pi/2$.

We introduce the index j' which is defined by the relations $-\pi/4 \leqslant \phi_{j'-1}$ and $\phi_i < -\pi/4$ for $i=j',\ldots,j$. Obviously, we have $\mathrm{Im}Y_i < 0$ and therefore $b_i + a_i - \omega[\mathrm{Im}(Y_i)/|Y_i|^2] > 0$ for $i=j', j'+1,\ldots,j$. Using (A14) and $\mathrm{Re}Y_{i-1} \geqslant 0$ (for all $i \leqslant j$), we obtain $\mathrm{Re}Y_i \geqslant \omega \mathrm{Im}Y_i/(a_i + b_i)$. This yields for $i=j',\ldots,j$,

$$\begin{aligned}
\phi_{i-1} - \phi_i &= \arctan\left(\frac{\omega - \omega \dfrac{\mathrm{Re}(Y_i)}{|Y_i|^2}}{b_i + a_i - \omega \dfrac{\mathrm{Im}(Y_i)}{|Y_i|^2}} \right) \\
&\leqslant \arctan\left(\frac{\omega - \dfrac{\omega^2 \mathrm{Im}(Y_i)}{(b_i + a_i)|Y_i|^2}}{b_i + a_i - \omega \dfrac{\mathrm{Im}(Y_i)}{|Y_i|^2}} \right) \\
&= \arctan\left(\frac{\omega}{a_i + b_i} \right) < \frac{\omega}{a_i + b_i}.
\end{aligned} \tag{A15}$$

Now we have to distinguish two different cases:

(i) $j' \geqslant 2$. By summing the inequality (A15) from $i=j'$ to $i=j$ and then taking into account the definitions of j and j', we find

$$-\frac{\pi}{4} + \frac{\pi}{2} < \phi_{j'-1} - \phi_j < \sum_{i=j'}^{j} \frac{\omega}{a_i + b_i} = \frac{\omega(j-j'+1)\nu A_{j'}}{v_l}, \tag{A16}$$

where definition (A7) has been used. The property $\omega \leqslant c_1$ then implies

$$j-1 \geqslant j-j'+1 > \frac{\pi v_l}{4A_{j'}\nu c_1}. \tag{A17}$$

(ii) $j'=1$: This means that $\phi_1 < -\pi/4$ and according to Eq. (A13), $\omega < -b_1 = |b_1|$. Now we sum the inequality (A15) from $i=2$ to $i=j$ and then use the expression $\arctan x > \pi x/4$ for $0<x<1$, thereby obtaining

$$\frac{\pi\omega}{-4b_1} < \arctan\left(\frac{\omega}{-b_1}\right) = \arctan\left(\frac{b_1}{\omega}\right) + \frac{\pi}{2}$$

$$< \phi_1 - \phi_j < \frac{\omega\nu(j-1)A_2}{v_l}. \tag{A18}$$

Therefore we find with Eq. (A4):

$$j-1 > \frac{\pi v_l}{4\,\nu A_2 |b_1|} \geqslant \frac{\pi v_l}{4\,A_2 \nu c_1}. \tag{A19}$$

Putting together (A17) and (A19) we obtain the inequality (A6).

(b) Let now $\omega > c_1$: To prove the inequality (A8), we shall define the auxiliary functions,

$$Z_i = Y_i - \frac{\lambda}{\lambda + b_i}. \tag{A20}$$

These functions solve the following discrete equation,

$$(\lambda + a_i + b_i)Z_i - a_i Z_{i-1} = \lambda a_i \left(\frac{1}{\lambda + b_{i-1}} - \frac{1}{\lambda + b_i}\right), \tag{A21}$$

with the boundary condition $Z_1 = 0$. The solution of this problem is

$$Z_n = \sum_{k=2}^{n} \frac{\lambda(b_k - b_{k-1})}{(\lambda + b_{k-1})(\lambda + b_k)} \prod_{i=k}^{n} \frac{a_i}{\lambda + b_i + a_i}. \tag{A22}$$

As all b_i are real quantities, we have $|i\omega + b_i| > \omega$ and obtain the following inequality for $|Z_j|$ by using the preceding formula with $\lambda = i\omega$, $\omega > 0$:

$$|Z_j| < \frac{1}{\omega} \sum_{k=2}^{j} |b_k - b_{k-1}| \prod_{i=k}^{j} \frac{a_i}{|b_i + a_i + i\omega|}. \tag{A23}$$

Now we have $|Z_j| > -\ \mathrm{Re} Z_j = -\ \mathrm{Re} Y_j + \omega^2/(\omega^2 + b_j^2) > \omega^2/(\omega^2 + b_j^2)$, where $\mathrm{Re} Y_j < 0$ and the definition of Z_n have been used. This inequality together with (A23) yield

$$\frac{\omega^3}{\omega^2 + b_j^2} < \sum_{k=2}^{j} |b_k - b_{k-1}| \prod_{i=k}^{j} \frac{a_i}{|b_i + a_i + i\omega|}. \tag{A24}$$

We now estimate the right side of (A24). The definition (23) of b_i and the mean value theorem yield

$$|b_k - b_{k-1}| < c_2 |E_k^c - E_{k-1}^c|. \tag{A25}$$

Equation (14) for the stationary state now yields $0 < E_k^c - E_{k-1}^c = (I^*/a_k - \nu)$, so that $0 < E_k^c - E_{k-1}^c < \nu(I^*/v_l - 1)$. Thus we can write

$$|b_k - b_{k-1}| < \nu\left(\frac{I^*}{v_l} - 1\right) c_2. \tag{A26}$$

On the other hand, as we are considering the case $\omega > c_1$, we find that

$$\frac{a_i}{|b_i + a_i + i\omega|} < \frac{a_i}{|b_i + a_i + i c_1|} \leqslant \mu, \tag{A27}$$

according to (A10). Inserting (A26) and (A27) into (A24), we obtain

$$\frac{\omega^3}{\omega^2 + c_1^2} < \nu c_2 \left(\frac{I^*}{v_l} - 1\right) \left(\sum_{k=2}^{j} \mu^{j-k+1}\right)$$

$$= \nu c_2 \left(\frac{I^*}{v_l} - 1\right) \mu \frac{\mu^{j-1} - 1}{\mu - 1}. \tag{A28}$$

Since $\omega > c_1$, $\omega^3/(\omega^2 + c_1^2) > c_1/2$. Inserting this into (A28), we obtain (A8). Therefore lemma 4 is proved.

Lemma 4 yields necessary conditions for the instability of a given stationary field profile $\{E_i^c\}$ corresponding to a fixed bias. We would like to obtain a general condition on ν, which should only depend on the $v(E)$ curve and the parameter c, but not on the specific stationary field profile. This can be achieved by the following considerations:

$$A_k = \frac{v_l}{(j-k+1)\nu} \sum_{i=k}^{j} \frac{1}{a_i + b_i} \leqslant \frac{v_l}{v_l - \nu c_1}. \tag{A29}$$

Therefore we have $A < v_l/(v_l - \nu c_1)$ from Eq. (A7), which inserted into the inequality (A6) gives

$$(j-1)\nu > \pi \frac{v_l - \nu c_1}{4c_1}. \tag{A30}$$

From the definition (A10) we obtain

$$\mu \leqslant \max_{E_l \leqslant E_i \leqslant E_h} \left\{\frac{a_i}{a_i - c_1}\right\} \leqslant 1 + \frac{\nu c_1}{v_l - \nu c_1}. \tag{A31}$$

This yields

$$B \leqslant \frac{v_l}{(j-1)\nu c_1} \left[\left(1 + \frac{\nu c_1}{v_l - \nu c_1}\right)^{j-1} - 1\right]$$

$$\leqslant \frac{v_l}{(j-1)\nu c_1} \left[\exp\left(\frac{(j-1)\nu c_1}{v_l - \nu c_1}\right) - 1\right] =: C, \tag{A32}$$

to be inserted in (A8). The result is

$$(j-1)\nu > \frac{v_l c_1}{2C(I^* - v_l)c_2}. \tag{A33}$$

We now use the obvious inequality $N \geqslant j$ in (A30) and (A33) thereby obtaining the condition (32) as a necessary condition for oscillatory instability of the steady state.

*Now at: Mikroelektronik Centret, Technical University of Denmark, DK-2800 Lyngby, Denmark.

[1] L. Esaki and L. L. Chang, Phys. Rev. Lett. **33**, 495 (1974).

[2] Y. Kawamura, K. Wakita, H. Asahi, and K. Kurumada, Jpn. J. Appl. Phys. **25**, L928 (1986).

[3] K. K. Choi, B. F. Levine, R. J. Malik, J. Walker, and C. G. Bethea, Phys. Rev. B **35**, 4172 (1987).

[4] P. Helgesen and T. G. Finstad, in *Proceedings of the 14th Nordic Semiconductor Meeting*, edited by Ole Hansen (University of Århus, Århus, 1990), p. 323.

[5] H. T. Grahn, R. J. Haug, W. Müller, and K. Ploog, Phys. Rev. Lett. **67**, 1618 (1991).

[6] S. H. Kwok, R. Merlin, H. T. Grahn, and K. Ploog, Phys. Rev. B **50**, 2007 (1994).

[7] J. Kastrup, H. T. Grahn, K. Ploog, F. Prengel, A. Wacker, and E. Schöll, Appl. Phys. Lett. **65**, 1808 (1994).

[8] R. Merlin, S. H. Kwok, T. B. Norris, H. T. Grahn, K. Ploog, L. L. Bonilla, J. Galán, J. A. Cuesta, F. C. Martínez, and J. M. Molera, in *Proceedings of the 22nd International Conference on the Physics of Semiconductors*, edited by D. J. Lockwood (World Scientific, Singapore, 1995), p. 1039.

[9] S.-H. Kwok, T. C. Norris, L. L. Bonilla, J. Galán, J. A. Cuesta, F. C. Martínez, J. M. Molera, H. T. Grahn, K. Ploog, and R. Merlin, Phys. Rev. B **51**, 10 171 (1995).

[10] H. T. Grahn, J. Kastrup, K. Ploog, L. L. Bonilla, J. Galán, M. Kindelan, and M. Moscoso, Jpn. J. Appl. Phys. **34**, 4526 (1995).

[11] J. Kastrup, R. Klann, H. T. Grahn, K. Ploog, L. L. Bonilla, J. Galán, M. Kindelan, M. Moscoso, and R. Merlin, Phys. Rev. B **52**, 13 761 (1995).

[12] A. A. Ignatov, V. I. Piskarev, and V. I. Shashkin, Fiz. Tekh. Poluprovodn. **19**, 2183 (1985) [Sov. Phys. Semicond. **19**, 1345 (1985)].

[13] B. Laikhtman, Phys. Rev. B **44**, 11 260 (1991).

[14] F. Prengel, A. Wacker, and E. Schöll, Phys. Rev. B **50**, 1705 (1994); **52**, 11 518(E) (1995).

[15] L. L. Bonilla, J. Galán, J. A. Cuesta, F. C. Martínez, and J. M. Molera, Phys. Rev. B **50**, 8644 (1994).

[16] D. Miller and B. Laikhtman, Phys. Rev. B **50**, 18 426 (1994).

[17] L. L. Bonilla, in *Nonlinear Dynamics and Pattern Formation in Semiconductors*, edited by F. J. Niedernostheide (Springer, Berlin, 1995), Chap. 1.

[18] A. Wacker, F. Prengel, and E. Schöll, in *Proceedings of the 22nd International Conference on the Physics of Semiconductors*, edited by D. J. Lockwood (World Scientific, Singapore, 1995), p. 1075.

[19] O. M. Bulashenko and L. L. Bonilla, Phys. Rev. B **52**, 7849 (1995).

[20] A. Wacker, G. Schwarz, F. Prengel, E. Schöll, J. Kastrup, and H.T. Grahn, Phys. Rev. B **52**, 13 788 (1995).

[21] A. N. Korotkov, D. V. Averin, and K. K. Likharev, Appl. Phys. Lett. **62**, 3282 (1993).

[22] A. N. Korotkov, D. V. Averin, and K. K. Likharev, Phys. Rev. B **49**, 1915 (1994).

[23] J. Kastrup, R. Hey, K. Ploog, H. T. Grahn, L. L. Bonilla, M. Kindelan, M. Moscoso, A. Wacker, and J. Galán, following paper, Phys. Rev. B **55**, 2476 (1997).

[24] O. M. Bulashenko, L. L. Bonilla, J. Galán, J. A. Cuesta, F. C. Martínez, and J. M. Molera, in *Quantum Transport in Ultrasmall Devices*, Vol. 342 of *NATO Advanced Study Institute, Series B: Physics*, edited by D. K. Ferry, H. L. Grubin, C. Jacoboni, and A. P. Jauho (Plenum Press, New York, 1995), p. 501.

[25] M. Patra, Studienarbeit, Technische Universität Berlin, 1995.

[26] G. Iooss and D. D. Joseph, *Elementary Stability and Bifurcation Theory* (Springer, New York, 1980).

[27] D. Dellwo, H. B. Keller, B. J. Matkowsky, and E. L. Reiss, SIAM J. Appl. Math. **42**, 956 (1982).

[28] A. Wacker and E. Schöll, J. Appl. Phys. **78**, 7352 (1995).

[29] S. H. Kwok, U. Jahn, J. Menniger, H. T. Grahn, and K. Ploog, Appl. Phys. Lett. **66**, 2113 (1995).

[30] L. L. Bonilla, M. Kindelan, M. Moscoso, and A. Wacker (unpublished).

[31] M. P. Shaw, H. L. Grubin, and P. R. Solomon, *The Gunn-Hilsum Effect* (Academic Press, New York, 1979).

[32] F. J. Higuera and L. L. Bonilla, Physica D **57**, 161 (1992).

[33] L. L. Bonilla, F. J. Higuera, and S. Venakides, SIAM J. Appl. Math. **54**, 1521 (1994).

[34] P. Guéret, Phys. Rev. Lett. **27**, 256 (1971).

[35] A. D. Martin, M. L. F. Lerch, P. E. Simmonds, and L. Eaves, Appl. Phys. Lett. **64**, 1248 (1994).

[36] A. Wacker and A.-P. Jauho, Superlatt. Microstruct. (to be published).